Supporting Information

Organic Photodetectors with High Detectivity for Broadband Detection Covering UV-Vis-NIR

Congdi Xu[a], Peng Liu[a], Chuang Feng[a], Zhicai He[a,b], Yong Cao[a]*

a, Institute of Polymer Optoelectronic Materials and Devices, State Key Laboratory of Luminescent Materials and Devices, South China University of Technology, Guangzhou 510640, China

b, Department of Physics, Imperial College London, London SW7 2BW, U.K

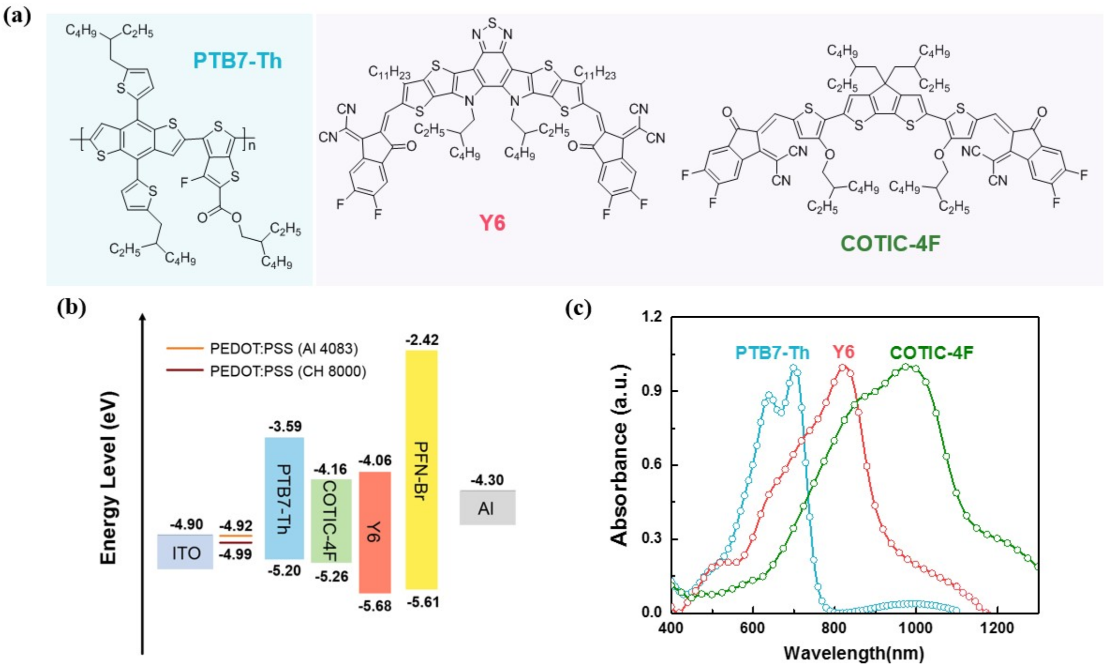

Fig. S1 (a) Chemical structures of the active layer materials: PBT7-Th, Y6 and COTIC-4F. (b) The energy level diagram of the materials employed in this work. (c) UV-Vis absorption spectra of the active layer materials as films.

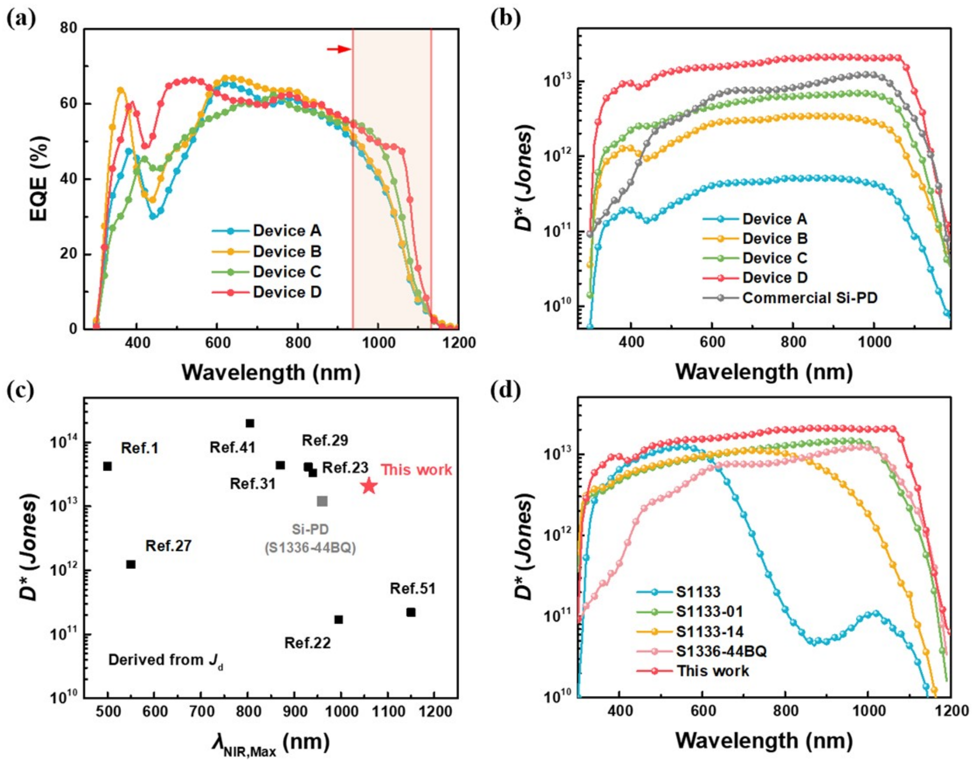

Fig. S2 (a) EQE profile (at -0.1 V) of devices with different architecture (the selected orange bar shows the wavelength region where the EQE spectrum has been gradually expanded after optimization). (b) The specific detectivity (D*) of OPDs derived from the J_d at -0.1 V. The gray curve represents the commercial Si PDs (Hamamatsu S1336-44BQ). (c) Shot-noise-limited specific detectivity (D*) as function of maximum wavelength at NIR region ($\lambda_{NIR,Max}$) accomplished in this work in comparison to previously reported OPDs and the commercial photodetectors with the same calculation method (see also Table S1). (d) Specific detectivity (D*) obtained from J_d of the optimal OPD in this work and four commercial Si PDs (Hamamatsu S1133, S1133-01, S1133-14, and S1336-44BQ).

Table S1. Performance parameters of peer OPDs, the optimal devices in this work and commercial Si PDs.

Active layer	Spectra region (nm)	Bias (V)	EQE (%)	R (A/W)	D^* (Jones)	LDR (dB)	f_{3dB} (kHz)	Ref.
PDDTT:$PC_{60}BM$	300-1450	-0.1	26%	0.17	4.2×10^{13} a) @500 nm	>100	NA	[1]
PM6:O4TFIC	400-1100	0	NA	0.50 @890 nm	9.0×10^{11} b) @915 nm	NA	>50	[17]
PBDTTT-C-T:FOIC	300-1000	-1	55% @730 nm	0.30 @900 nm	2.1×10^{13} b) @860 nm	106	30	[18]
PTB7-Th: COTIC-4F	300-1100	0	51% @960 nm	0.37 @950 nm	1.7×10^{11} a) @995 nm	NA	NA	[22]
PTB7-Th: CO1-4Cl	400-1100	-0.1	60-68% @ 750-940 nm	0.45 @940 nm	3.31×10^{13} a)/ >10^{12} b) @940 nm	126	240	[23]

P3HT:$PC_{71}BM$	300-700	-0.5	68.6% @545 nm	0.302 @550 nm	$1.23\times10^{12\ a)}$ @505 nm	NA	NA	[27]
PTB7-Th: IEICO-4F	300-1000	-0.1	>65% @ 580-930 nm	0.54 @930 nm	$5.1\times10^{13\ a)}$/ $4.6\times10^{13\ b)}$ @930 nm	157	4.5	[29]
NT40: IEICO-4F	300-1000	-0.1	57.2% @870 nm	0.40 @870 nm	$4.4\times10^{13\ a)}$/ $7.5\times10^{12\ b)}$ @870 nm	123	>100	[31]
PTB7-Th: CO_i8DFIC: $PC_{71}BM$	300-1000	0	NA	0.35 @670 nm	$5.6\times10^{11\ b)}$ @670 nm	135	~2	[32]
PTB7-Th: COTIC-4Cl:PCBM	300-1200	-0.1	>40% @1070 nm	0.35 @1070 nm	$5\times10^{12\ b)}$ @1070 nm	>120	>1000	[34]
D18:Y6	300-1000	0	>80% @805 nm	0.499 @805 nm	$1.97\times10^{14\ a)}$/ $1.14\times10^{13\ b)}$ @805 nm	83	NA	[41]
CPDT-TQ: $P_{71}BM$	600-1550	0	8% @1190 nm	NA	$5\times10^{10\ b)}$ @1190 nm	NA	NA	[43]
P1:$P_{71}BM$ (no gain)	300-1540	-0.1	7.8% @1200 nm	0.08 @1150 nm	$2.2\times10^{11\ a)}$ @1150 nm	NA	NA	[51]

PFT-OEHp:Y6	300-1000	-0.1	~80%	0.5 @800 nm	1.16×10^{13} b) @800 nm	>135	50	[65]
PTB7-Th: COTIC-4F:Y6	300-1200	-0.1	62.4% @780 nm	0.41 @1060 nm	2.1×10^{13} a)/ 6.9×10^{12} b) @1060 nm	102	45	This work
Si (S1336-44BQ)	300-1100	-0.1	72.8% @960 nm	0.57 @960 nm	1.2×10^{13} @960 nm	NA	NA	Commercial

a) The shot-noise-limited specific detectivity is calculated by the equation of $D^* = \frac{R}{\sqrt{2qJ_d}}$. b) The specific detectivity are obtained by the equation of $D^* = \frac{R\sqrt{A}}{S_n}$.

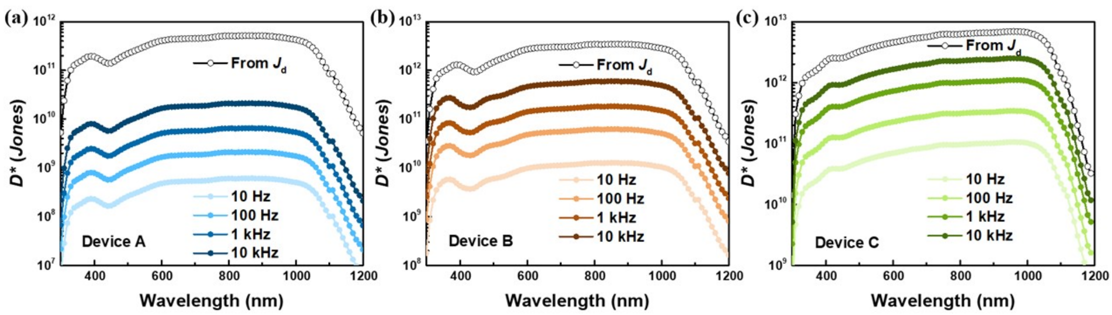

Fig. S3 The specific detectivity (D*) obtained by the equation of $D^* = \frac{R\sqrt{A}}{S_n}$ at the frequency of 10,100,1000,0000 Hz, respectively.

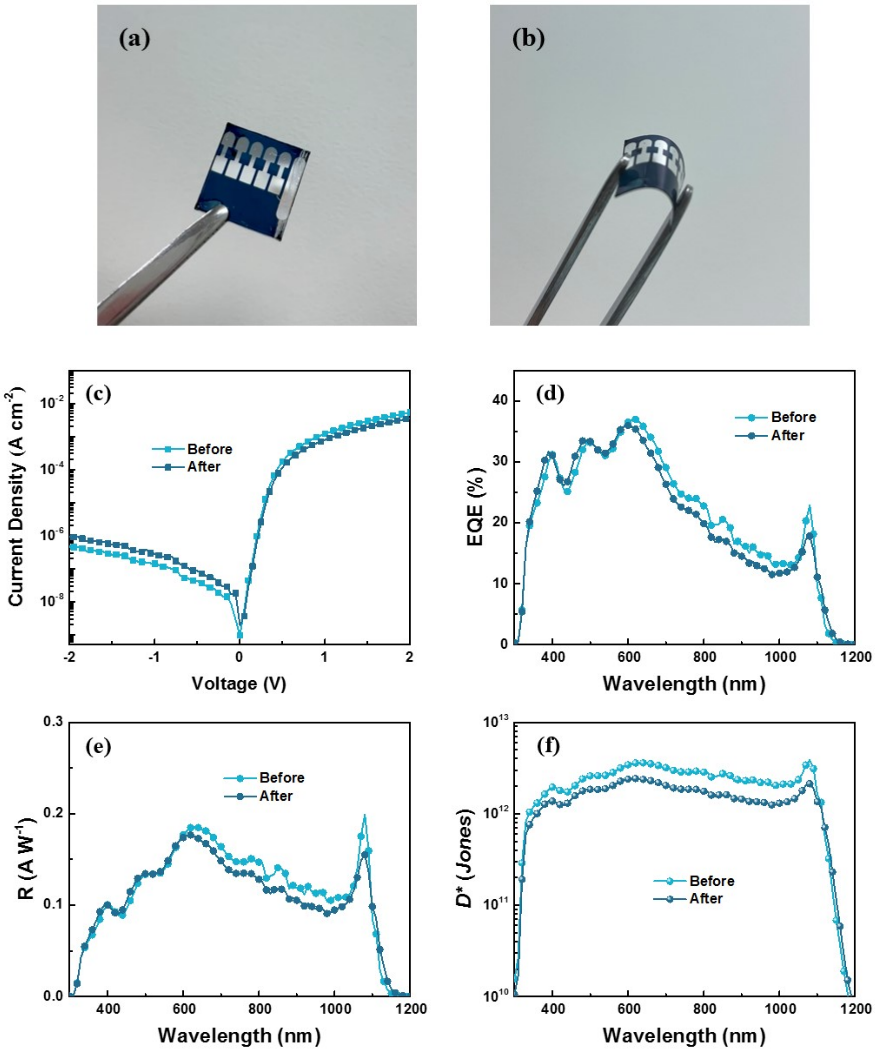

Fig. S4 (a-b) The picture and the characteristics of flexible device before and after bending. (c-f) device performance of the flexible device before and after bending.

Table S2. Performance parameters of flexible OPDs before and after bending.

Flexible OPDs	J_d @-0.1 V (A/cm^2)	Rectification ratios (±2 V)	EQE (%)	R (A/W)	D^*_{max} (Jones)
Before bending	8.3×10^{-9}	1.2×10^{4}	22.8	0.20	3.9×10^{12}
After bending	2.1×10^{-8}	3.9×10^{3}	17.8	0.16	2.0×10^{12}

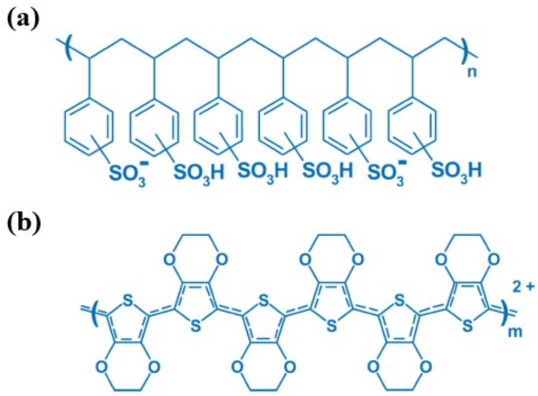

Fig. S5 Chemical structures of the (a) PSS^- and (b) $PEDOT^+$ chains.[1]

Table S3. Parameters of two kinds of PEDOT:PSS.

Typical Property or Characteristic	pH at 20° C	$PEDOT^+/PSS^-$ ratio	Resistivity (Ohm/cm)	Mean WF (mV)
Al 4083	1.7 – 2.3	1:6	500 – 5000	525.3 mV
CH 8000	1.2 – 1.8	1:20	1×10^5 – 3×10^5	591.8 mV
ITO	/	/	/	506.2 mV

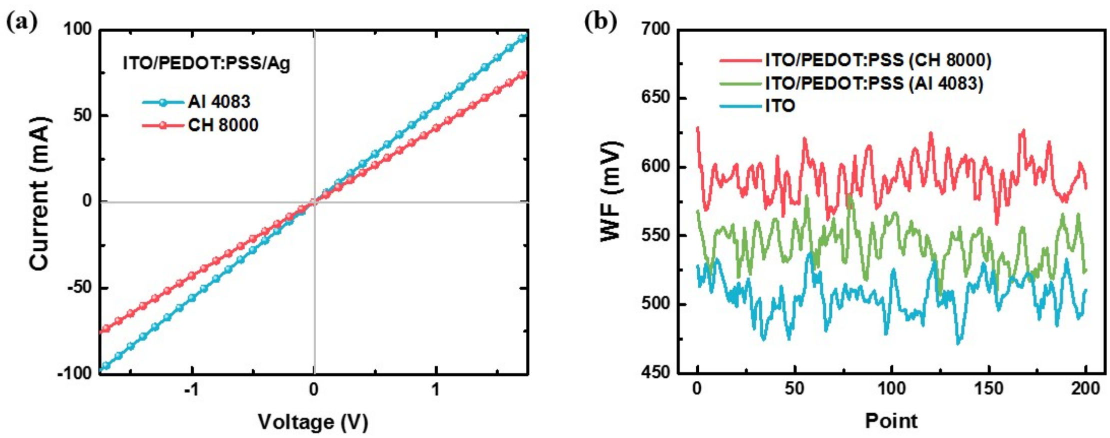

Fig. S6 (a) Current-Voltage curve of ITO/Interlayer/Ag devices. (b) Work function diagram of film location points measured by SKPM.

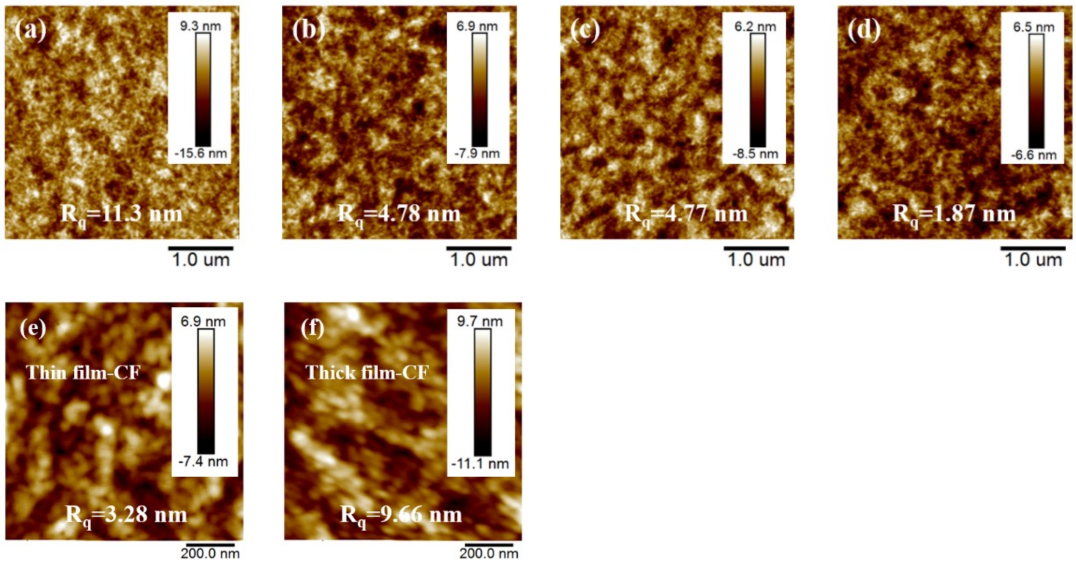

Fig. S7 The AFM height images of the films, (a) PEDOT:PSS (Al4083) /PTB7-Th:COTIC-4F (120 nm), (b) PEDOT:PSS (CH8000) /PTB7-Th:COTIC-4F (120 nm), (c,e) PEDOT:PSS (CH8000) /PTB7-Th:COTIC-4F:Y6 (120 nm) and (d,f) PEDOT:PSS (CH8000) /PTB7-Th:COTIC-4F:Y6 (300 nm). The active layers (PTB7-Th:COTIC-4F:Y6) of (e) and (f) use chloroform as solvent, others use chlorobenzene as solvent.

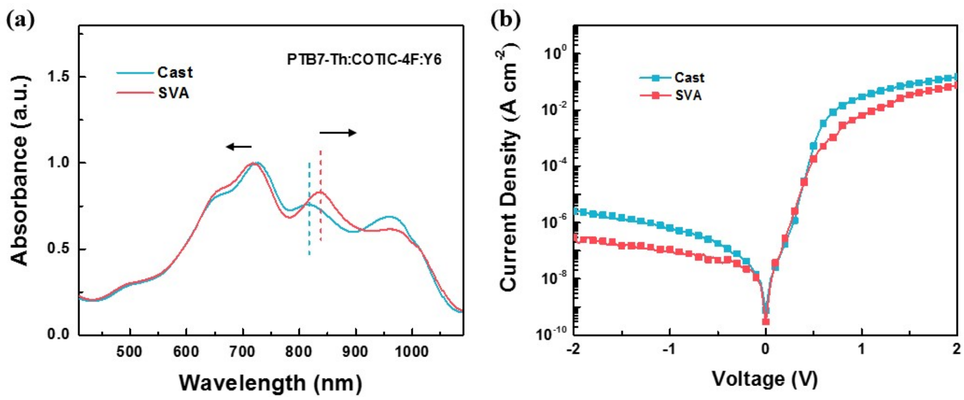

Fig. S8 The absorption spectra of the ternary films and the J_d-V curve of the devices derived from the films before and after solvent vapor annealing.

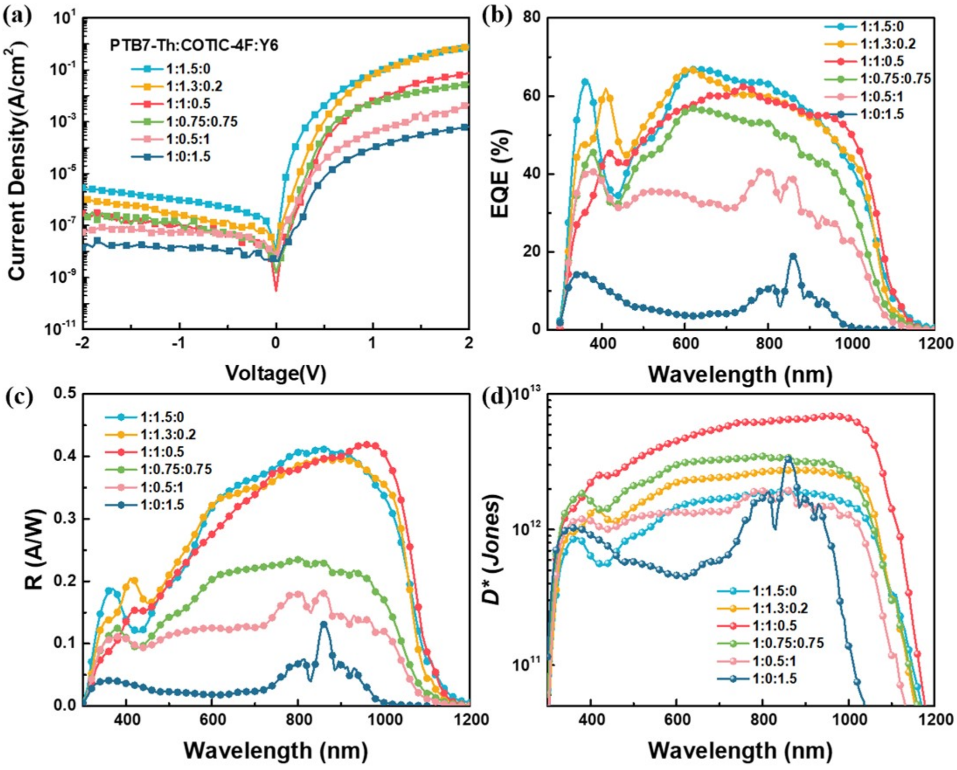

Fig. S9 The performance of the devices with different proportions of PTB7-Th:COTIC-4F:Y6 (wt:wt).

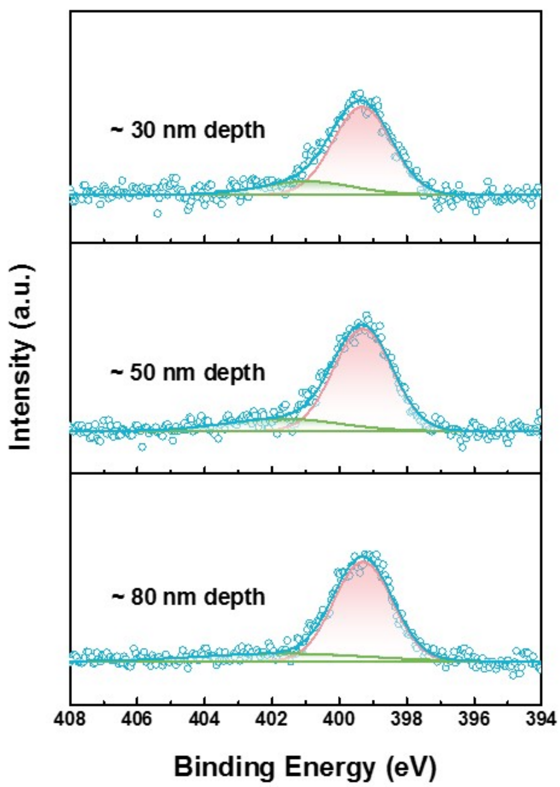

Fig. S10 The XPS profile of N 1s spectrum of ternary blend film (PTB7-Th:COTIC-4F:Y6) at different etching depths. The peaks in green could be produced by Y6.

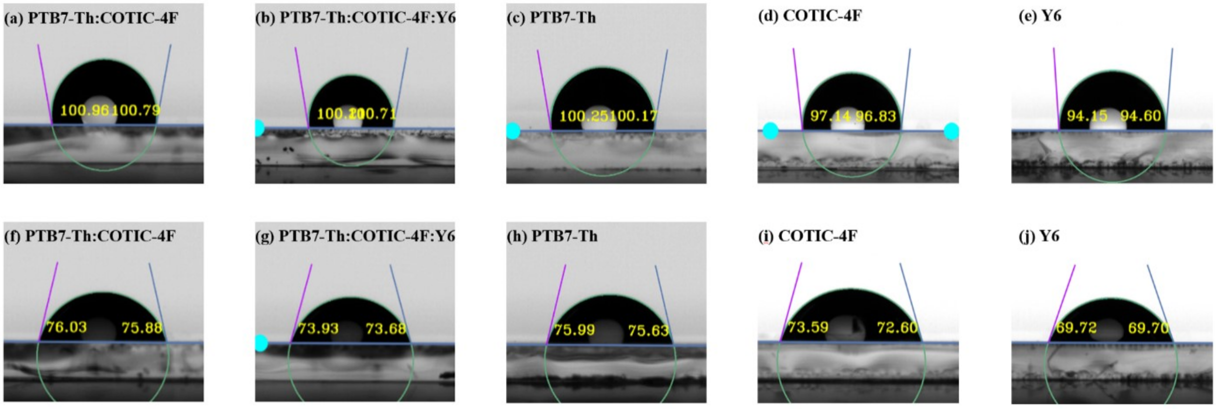

Fig. S11 Views of surface contact angle measurements with the blend and pure films. The measurements are carried out by using deionized water (a-e) and diiodomethane (f-j) as the wetting liquid.

Table S4. The Parameters of the films obtained from contact angle measurement

Film	γ [a)] (mN·m^{-1})	γ_d (mN·m^{-1})	γ_p (mN·m^{-1})	θ_{wat} (°)	θ_{oil}(°)	δ (MPa$^{1/2}$)	Δδ [b)] (MPa$^{1/2}$)
PTB7-Th: COTIC-4F	16.82	13.84	2.98	100.88	75.96	/	/
PTB7-Th: COTIC-4F:Y6	17.76	15.10	2.66	100.46	73.81	/	/
PTB7-Th	16.53	13.24	3.29	100.31	75.81	14.91	/
COTIC-4F	18.32	14.31	4.02	96.99	73.01	15.70	0.79
Y6	20.01	15.42	4.58	94.38	69.71	16.41	1.49

a) Calculated by Owens-Wendt-Rabel-Kaelble (OWRK) method

b) $\Delta\delta=|\delta_{donor} - \delta_{acceptor}|$

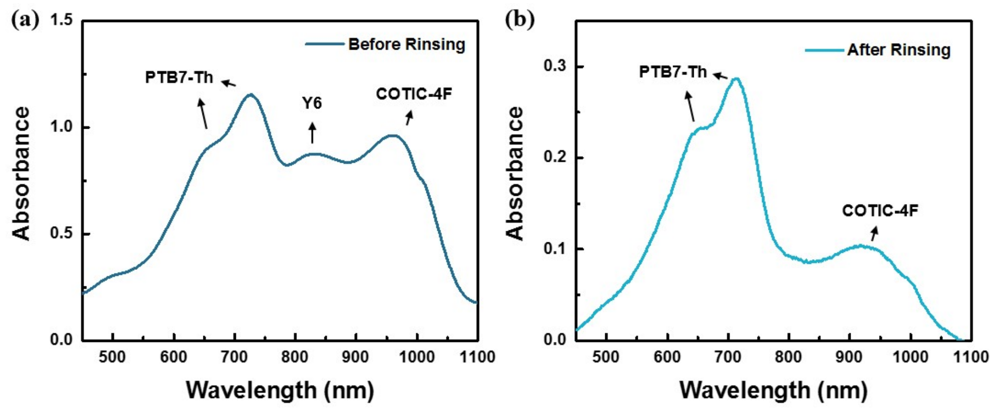

Fig. S12 The absorption spectra of the film (active layer) before and after solvent rinsing. It can be seen from the spectrum that Y6 is almost completely washed away, which proves that Y6 is mainly concentrated on the surface.

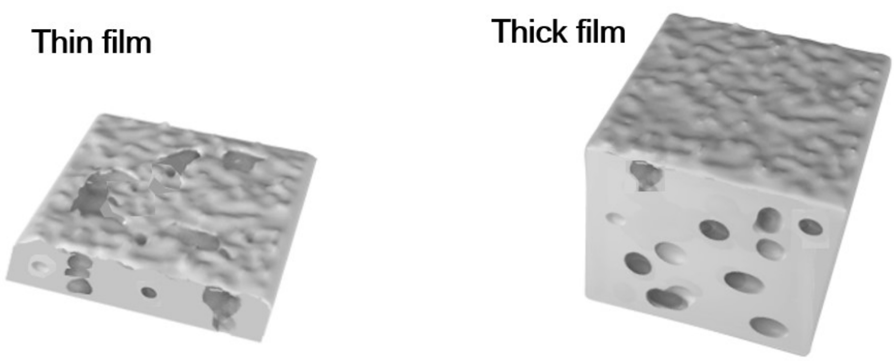

Fig. S13 The schematic diagram of pathways formed inside the thin film and thick film.

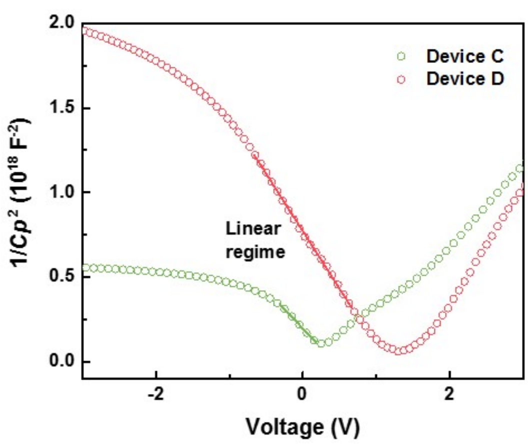

Fig. S14 The $1/Cp^2$-V characteristics of devices measured at a frequency of 1 kHz.

Table S5. The results of Mott-Schottky analysis of the OPDs with different thickness.

Thickness of devices	The charge doping density (*N*)
120 nm	3.20×10^{16} cm^{-3}
300 nm	2.15×10^{16} cm^{-3}

The relative permittivity of organic material is set to be 3.

The temperature-dependent dark current measurements were carried out to verified the surface trap state features by studying the activation energy (Ea) from the slope of Arrhenius plots (Chinese Phys. B 29, 098801 (2020)) as shown in Figure S15. For the device with thin film, the dark current J_0 shows 2 sets of Gaussian distributions, which may be attributed to the more complicated distribution of the surface trap states.

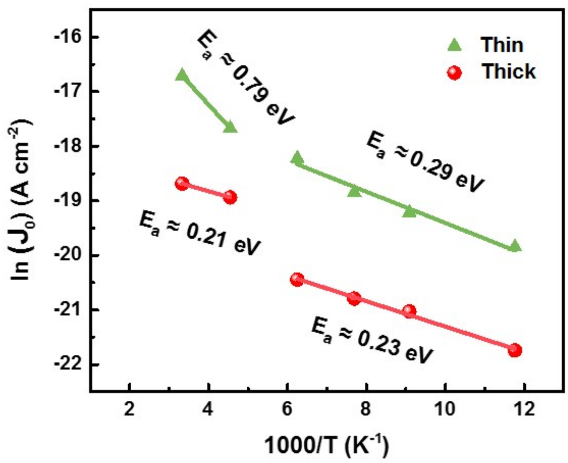

Fig. S15 The surface trap Gaussian distributions of the device deduced from temperature-dependent dark current measurements.

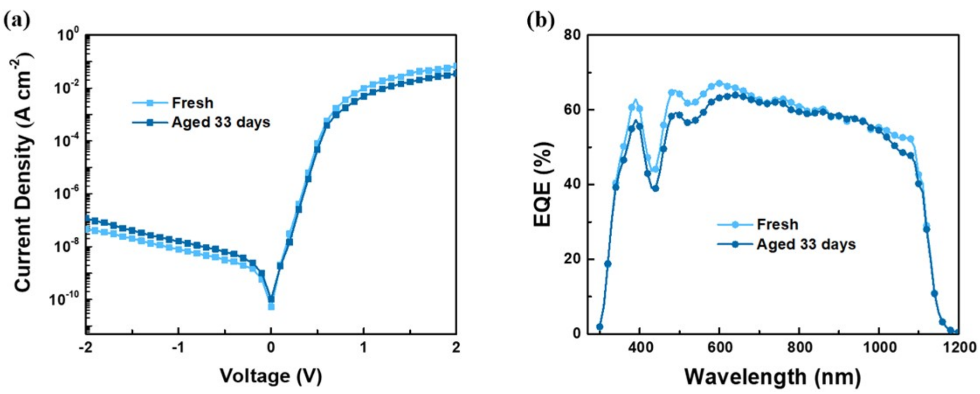

Fig. S16 The Dark *J-V* characteristics and EQE spectrum of optimized device before and after being stored in air for 33 days.

References

[1] https://www.heraeus.com/media/media/hec/documents_hec/brochures_en/CLEVIOS_FL_Innovate.pdf for "*CLEVIOS*™ PEDOT Conductive Polymers" (accessed: May 2021).